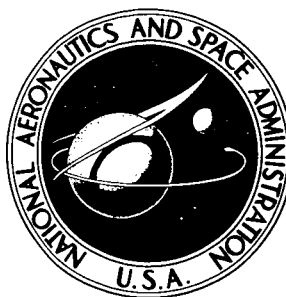


NASA TECHNICAL NOTE



NASA TN D-2803

NASA TN D-2803

FACILITY FORM 602

| | |
|-------------------------------|------------|
| N65 24375 | |
| (ACCESSION NUMBER) | (THRU) |
| 35 | 1 |
| (PAGES) | (CODE) |
| | 28 |
| (NASA CR OR TMX OR AD NUMBER) | (CATEGORY) |

AN ELECTROLYTIC TANK ANALOG FOR TWO-DIMENSIONAL ANALYSIS OF ELECTROSTATIC-THRUSTOR OPTICS

by John F. Staggs
Lewis Research Center
Cleveland, Ohio

GPO PRICE \$ _____

OTS PRICE(S) \$ 2.00

Hard copy (HC) _____

Microfiche (MF) 50

AN ELECTROLYTIC TANK ANALOG FOR TWO-DIMENSIONAL
ANALYSIS OF ELECTROSTATIC-THRUSTOR OPTICS

By John F. Staggs

Lewis Research Center
Cleveland, Ohio

NATIONAL AERONAUTICS AND SPACE ADMINISTRATION

For sale by the Clearinghouse for Federal Scientific and Technical Information
Springfield, Virginia 22151 - Price \$2.00

AN ELECTROLYTIC TANK ANALOG FOR TWO-DIMENSIONAL ANALYSIS OF ELECTROSTATIC-THRUSTOR OPTICS

by John F. Staggs

Lewis Research Center

SUMMARY

24375

An electrolytic tank analog used for two-dimensional analyses of electrostatic-thruster ion optics is described in detail. This analog has unique features that increase the ease of operation and versatility beyond previously reported designs. A generalized procedure, which permits a wide variety of space-charge-flow problems to be solved quickly and accurately, is used for space-charge simulation.

Solutions are given for operational problems encountered in the practical use of the analog, and some analyses of specific thruster accelerator configurations are presented to illustrate procedures and important applications of the analog. The use of the analog as a precursor to a more accurate digital computer analysis is recommended to speed up the initial investigation of a thruster configuration.

AUTHOR ↑

INTRODUCTION

Many of the problems associated with electrostatic thrusters have been solved. The focus of attention is turning toward lifetime extension (ref. 1). To maximize the operating lifetime of a thruster, the electrode system must be designed so that the ion beam does not intercept the accelerator electrode (see fig. 1).

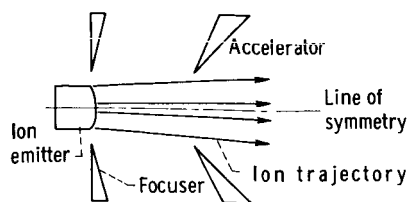
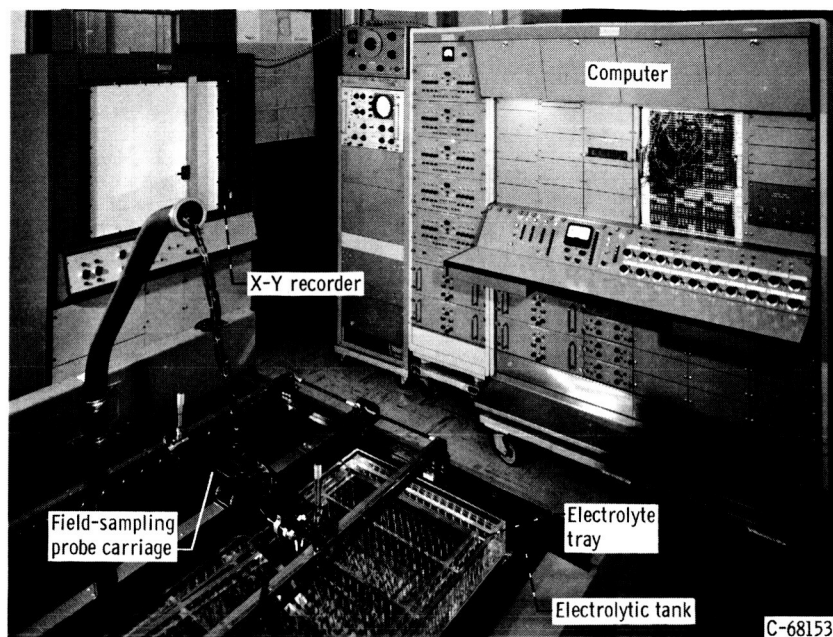
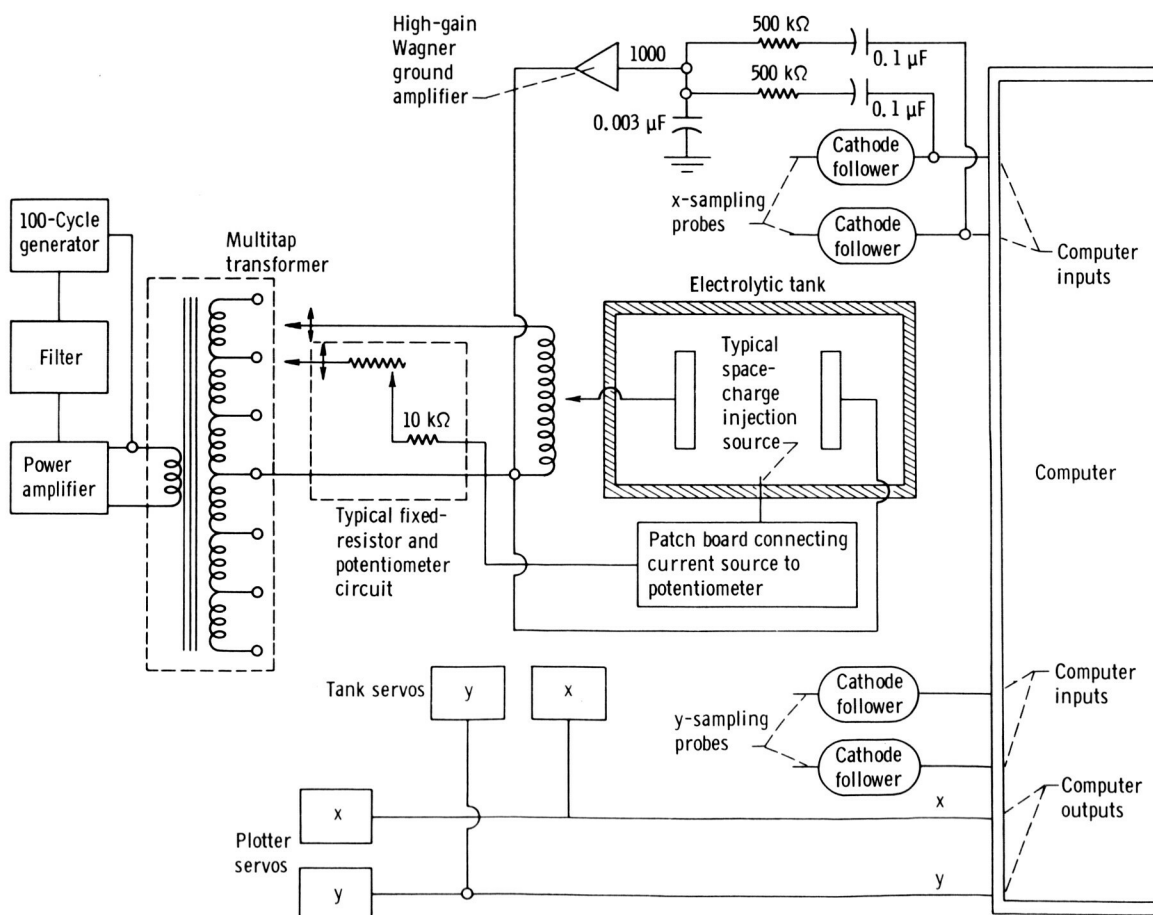


Figure 1. - Cross-sectional diagram of electrostatic thruster.

The width and shape of the ion beam in a thruster is a result of the combined effects of the space charge and the electrode shapes. Analyzing the space-charge flow for a wide variety of thruster configurations can be relatively simple and fast if an analog is available that is sufficiently versatile, accurate, and convenient to use. Digital computer programs exist for analyzing space-



(a) Overall view.



(b) Diagram of basic electrical system.

Figure 2. - Electrolytic tank analog.

charge flow in considerable detail, but an electrolytic tank analog is more appropriate for initial investigations of thruster configurations. Ions produced by charge exchange can also be treated readily with the electrolytic tank so that it is possible to estimate electrode erosion and lifetime (ref. 2).

The electrolytic tank analog discussed in this report is based on a design procured by Lewis from Hughes Research Laboratory. As will be shown, however, the equipment and techniques reported herein have been developed and extended to permit the solution of a wider variety of space-charge-flow problems in a shorter time. Along with a discussion of these solutions and the methods used to obtain them, this report describes the basic considerations involved in the design and operation of the analog. Sample calculations used in the operation of the analog are provided.

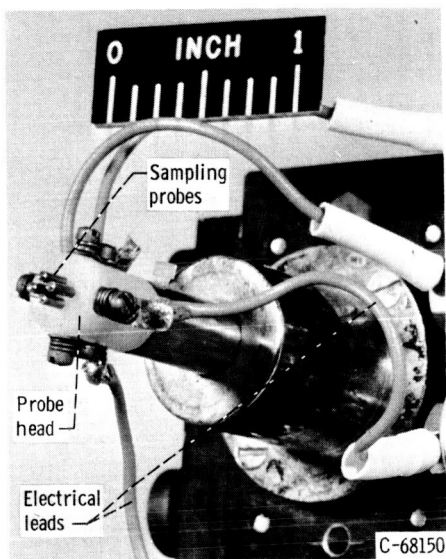
APPARATUS AND PROCEDURE

The plans and procedures for the original electrolytic tank analog at Lewis Research Center were procured from Hughes Research Laboratory. The present Lewis Research Center analog consists of the electrolytic tank, an analog computer, and a large X-Y recorder for obtaining permanent records of the results (fig. 2(a)). This analog has, since procurement, been considerably modified in both equipment and procedures. A basic electrical diagram of the system is shown in figure 2(b).

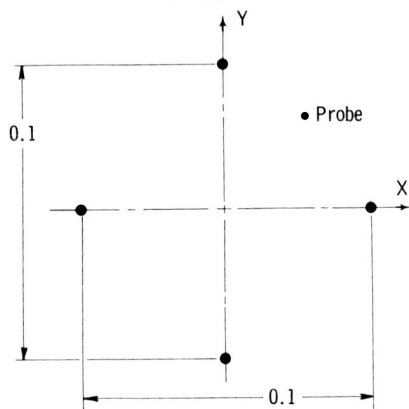
To simulate the thruster for the analog investigation, scale-model electrodes and an ion-emitting surface are placed in a plastic tray filled with electrolyte. For symmetrical designs, only half the thruster configuration need be considered. Voltages applied to the model electrodes establish electric fields throughout the electrolyte, and the space charge due to ion flow is simulated by means of "current" injection pins located in the tray (refs. 3 and 4).

The space-charge-flow problem involves, of course, the solution of Poisson's equation ($\nabla^2 V = \rho/\epsilon_0$) subject to the initial and boundary conditions of the particular case. (Symbols are defined in appendix A.) The equations of motion for the two-dimensional problems are

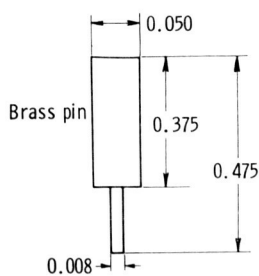
$$\text{and } \left. \begin{aligned} \frac{d^2 x_r}{dt^2} &= -\eta E_{x,r} \\ \frac{d^2 y_r}{dt^2} &= -\eta E_{y,r} \end{aligned} \right\} \quad (1)$$



(a) Sampling probe head.



(b) Sampling probe pin spacing.



(c) Sampling probe pin.

Figure 3. - Field-sampling probe details.
(All dimension in inches.)

where $\eta = q/m$ is the charge-to-mass ratio of the ions, $E_{x,r}$ and $E_{y,r}$ are the x- and y-components of the electric field intensity, and the subscript r refers to the real thruster. The equations of motion for a similar particle in the analog model are obtained by dimensional and time scaling so that, for the model thruster,

$$\left. \begin{aligned} \frac{d^2 x_m}{d\tau^2} &= -\eta E_{x,m} \\ \frac{d^2 y_m}{d\tau^2} &= -\eta E_{y,m} \end{aligned} \right\} \quad (2)$$

where x_m and y_m are the scaled model dimensions, τ is the scaled time, and $E_{x,m}$ and $E_{y,m}$ are the scaled electric field components set up in the electrolyte by the model. Equations (1) and (2) are of the same form and may be treated in the same manner. To begin the solution, the space-charge-free electric fields are used as the first approximation to the solution of the space-charge-flow problem, and ion trajectories are determined under these conditions. These trajectories provide a means of estimating a charge distribution from which a better approximation for the trajectories may be determined. By continuing this iterative process, convergence to the solution of Poisson's equation is obtained. In actual operation, the x- and y-components of the field intensity, measured at the surface of the electrolyte by a set of sampling probes, are fed to an analog computer for the solution of the equations of motion. The sampling probe carriage, driven by the computer output, traces out ion trajectories. The X-Y recorder shown in figure 2 is synchronized with the probe carriage and pro-

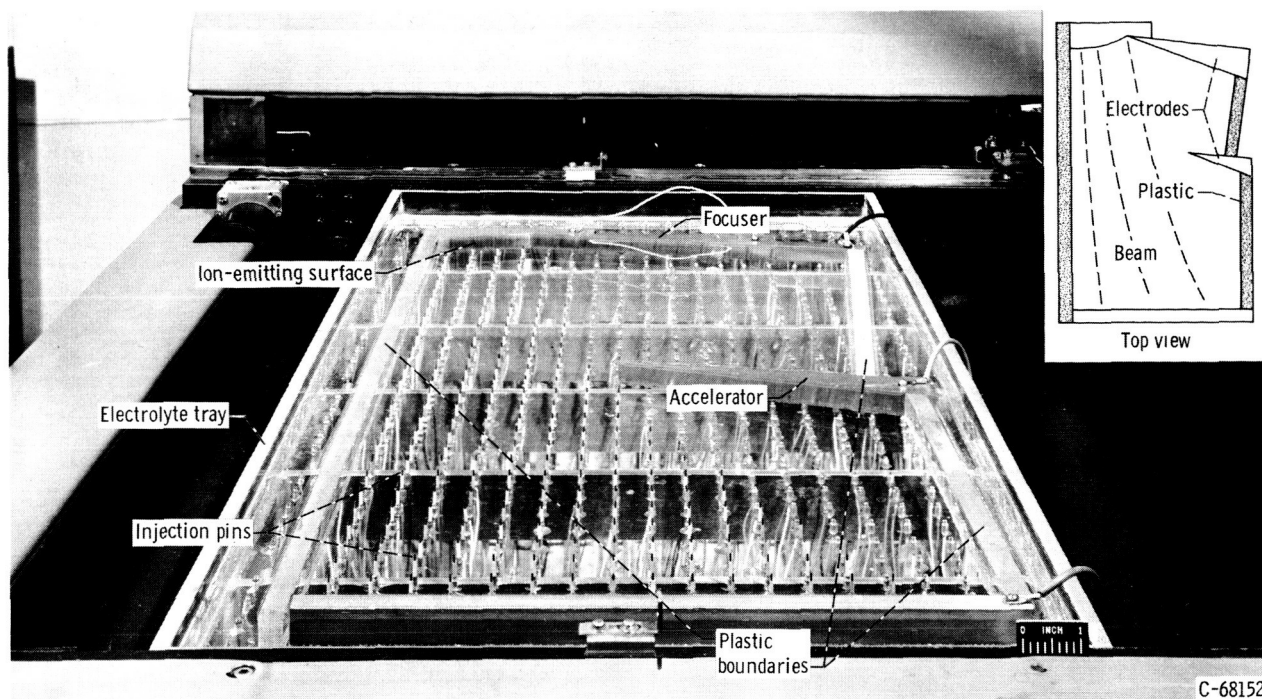


Figure 4. - Divergent-flow model electrodes in tank.

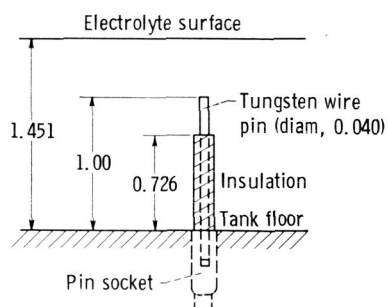


Figure 5. - Current-injection pin. (All dimensions in inches.)

vides a permanent record of the trajectories. Figure 3(a) is a photograph of the underside of the field-sampling probe. The probe details will be discussed in the section Field-Sampling Probe.

Electrolyte Tray and Current-Injection Pins

The plastic electrolyte tray is approximately 16 inches wide, 30 inches long, and 2 inches deep. The floor of the tray is accurately leveled by adjustments at its supports. Small sockets sealed in the floor of the tray provide receptacles for removable current-injection pins (see figs. 4 and 5). This unique feature permits the pins to be plugged in or removed as needed. There are several advantages of this removable-pin design compared with a permanent-pin design. The model electrodes do not require holes in them to fit over the pins. Cleaning the floor of the tray is much easier, and most important, electrode configurations may be changed quickly. Although trays exist in which the pins are secured by screws from the underside of the tray floor, the plug-in pins are more convenient to use. A patch-panel system (fig. 6) is used to connect each current-injection pin to a potentiometer and a series resistor. By adjusting the potentiometer and monitoring the voltage dropped across the resistor, the injection current of each pin may be set. The calcula-

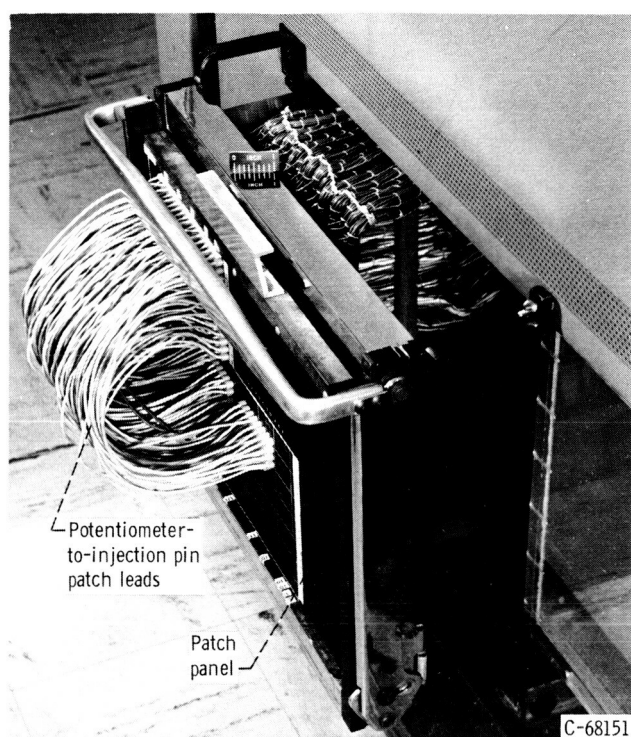


Figure 6. - Current-injection patch panel.

tion of the value of this current will be discussed in the section Obtaining Working Equations for Analog. Samples of the calculation are provided in appendix B.

Field-Sampling Probe

A photograph of the field-sampling probe is shown in figure 3(a) (p. 4). The probe head is attached to a micrometer screw so that the probe may be lowered into the electrolyte to a precise depth. The probe head consists of a nylon mounting block with four small gold-plated brass pins protruding from the underside. The brass sampling pins are held in locating holes in the nylon block by set screws. Electrical connections to the pins are made through the set screws. The pins form a square array (fig. 3(b)) with the diagonally opposite pins spaced $1/10$ inch apart. One of the brass pins is shown in detail in figure 3(c). References 5 to 7 discuss probe spacing and the effects of meniscus on the accuracy of electrolytic tank analogs. In principle, the closer the pin spacing is, the more accurate the field sampling will be; however, the distortion due to the meniscus about the pins may overshadow the increased accuracy due to closer spacing.

Associated Circuitry and Components

A power amplifier, driven by a 100-cycle-per-second sine-wave generator, delivers power to a transformer (fig. 2(b), p. 2). The model electrode potentials and the bias voltages of the current-injection pins are obtained from the multitap secondary of this transformer. Alternating-current voltages rather than direct-current voltages are used to reduce the battery action or polarization that occurs between electrodes.

The cathode followers (fig. 2) have a high input impedance to minimize current flow through the field-sampling probe pins; thus, field distortion by the pins is prevented. The output of the x-cathode followers is fed through a Wagner grounding circuit (fig. 2(b) and ref. 8). The output of the Wagner ground amplifier is then fed back to the model electrodes. As the probes move through the electrolyte, the output of the Wagner ground amplifier varies in such a way so as to maintain an electrical ground nearly midway between the two x-probes, thereby reducing capacitive effects at the probes. This results in a shifting in the values of the electrode reference potentials; however, the net potential difference between them remains unchanged. The values of the amplifier input capacitor and the amplifier gain of the Wagner ground circuit are adjusted so that the amplifier will remain stable at as high a gain as possible. For the analog reported herein, the maximum stable gain of the amplifier is about 1000.

The outputs of the x-cathode followers are also fed to the analog computer where their difference is determined and multiplied by an alternating-current reference signal, and the result is filtered to yield a direct-current signal. The magnitude of this signal is proportional to the field intensity E_x . The same operations of finding the difference, multiplying by a reference signal, and filtering are performed on the outputs of the y-cathode followers, and the two components of the equations of motion are solved simultaneously by the computer.

The circuit used for obtaining the difference, multiplying by the reference signal, and filtering (see fig. 7) eliminates the accessory equipment used in other analogs for this purpose (e. g., ref. 7). Computer components are used exclusively. The operation is as follows: for the signals from each pair of probes, the difference is obtained by inverting the sign (shifting the phase by 180°) of one and adding that result to the other signal. The resulting signal is a sinusoidal function $A_1 \sin \omega t$ where A_1 is the amplitude, ω is the frequency, and t is the time. By using an electronic multiplier, a reference signal is then multiplied by this function. The reference signal may be of the form $A_2(\omega t + \theta)$ where θ is the difference in phase between the working and the reference signals. The resultant product is then

$$[A_1 \sin \omega t][A_2 \sin(\omega t + \theta)] = \frac{A_1 A_2}{2} \cos \theta - \frac{A_1 A_2}{2} \cos(2\omega t + \theta) \quad (3)$$

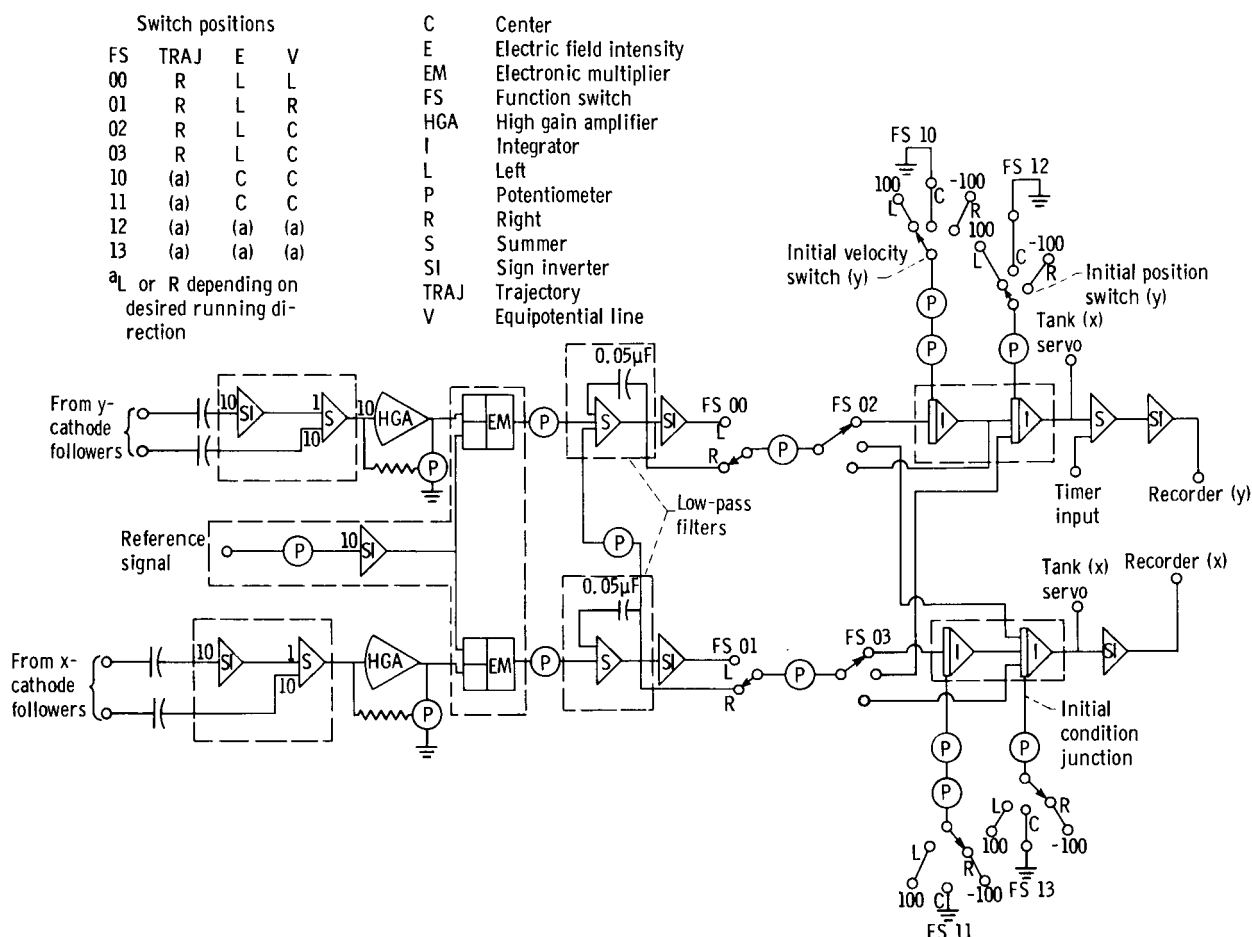


Figure 7. - Block diagram for analog computer program.

The first term of the product is a constant for any given phase difference, while the second is a sinusoidal signal of twice the original frequency. The low-pass filter circuit (fig. 7) allows only the constant portion of the product to be passed. This direct-current signal is proportional to the electric field strength component. Simultaneous double integration of these field components in the computer circuit yields the trajectory of a particle. The outputs of the double integration are used to drive simultaneously the x- and y-servosystems in the electrolytic tank, which propel the probe.

If the equations of motion are electronically integrated simultaneously by the computer only once and the computer outputs are plotted one against the other, the results are electric field lines. By reversing the plotter inputs, lines normal to the electric fields (equipotential lines) are plotted (ref. 7). If the gradient throughout an area is extremely small, the analog may not be able to plot the potential field accurately. In this case, the field must be plotted manually point by point.

Calibration

Before use, it is necessary to calibrate the analog. As mentioned previously, the four field-sampling probes are arranged to form the corners of a square (fig. 3(b), p. 4). Perfect alinement of these probes is practically impossible. Small deviations can be compensated for, however, by an electrical correction made to the signal measured by one pair of probes. This is done by adding part of the signal from one pair to the other so that both signals are the same under identical field conditions. Of course, the greatest degree of accuracy is obtained when the correction signal is very small. It is therefore necessary to aline the probes with care. In running an actual problem, the accuracy of the analog is also improved if the correction signal is taken from the pair of probes that are normal to the general direction of the trajectories.

Electrolyte and Model Electrodes

Two important factors that affect the amount of injection current are the conductivity σ of the electrolyte and the value of the fixed resistors (fig. 2, p. 2) in series with the injection pins. These two factors are independent of the model configuration and must be adjusted so that the desired range of currents can be injected with the power supply that is used. In the present analog, ordinary tap water having a conductivity of from 2.0×10^{-2} to 4.0×10^{-2} mho per meter is used for the electrolyte. The fixed resistors have a resistance of 10 000 ohms. The electrode material used for the models is stainless steel. Details of tests that were made to evaluate various materials are presented in appendix C.

Initial Conditions

Because of physical limitations imposed by the size of the sampling probe, trajectories to be traced are started about 3/16 inch from the simulated emitter. Because of this limitation, the simulated charged particles must be given an initial velocity that corresponds to the velocity a real particle would have in the field at that location. This condition may be set by applying the initial velocity in terms of voltage, at the initial condition junction of the velocity integrators (see fig. 7).

Spacing of Current-Injection Pins

The most accurate simulation of a space-charge field is accomplished by using the smallest injection-pin mesh spacing possible. A practical limitation, however, is the number of calculations and settings required to determine the pin currents from iteration to iteration. Because of the complex network of resistances between pins in the tank, some pin currents change as others are set. When a large number of pins are used, they may require resetting as many as three times for each iteration. The mesh size found suitable for a variety of problems was 0.8 inch. The number of pins used in the problems described in the section ILLUSTRATIVE EXAMPLES ranged from 25 to over 200.

THEORY

Space-Charge Simulation

The relation between the electric field and the charge density in a thruster is given by Poisson's equation in the form

$$\vec{\nabla}_r \cdot \vec{E}_r = \frac{\rho_r}{\epsilon_0} \quad (4)$$

where E_r is the electric field and ρ_r is the charge density in the real thruster. Define

$$\alpha \equiv \frac{E_r}{E_m} \quad (5)$$

where E_m is the electric field in the electrolytic model. If the model is scaled such that

$$\left. \begin{aligned} x_m &= Fx_r \\ y_m &= Fy_r \\ z_m &= Fz_r \end{aligned} \right\} \quad (6)$$

it follows that

$$\vec{\nabla}_m \cdot \vec{E}_m = \frac{\rho_r}{\epsilon_o \alpha F} \quad (7)$$

where F is the scale factor from equation (6). The relation between the current density and electric field in the electrolyte model is given by

$$\vec{j}_m = \sigma \vec{E}_m \quad (8)$$

where σ is the conductivity of the electrolyte. By substitution, equation (7) becomes

$$\vec{\nabla}_m \cdot \vec{j}_m = \frac{\sigma \rho_r}{\epsilon_o \alpha F} \quad (9)$$

By applying Gauss' law and including the scaling factors of equation (6), equation (9) becomes

$$\int_{V_m} \vec{\nabla}_m \cdot \vec{j}_m dv_m = \int_{S_m} \vec{j} \cdot \vec{ds}_m = \frac{\sigma F^2}{\epsilon_o \alpha} Q_r \quad (10)$$

where Q_r is the charge in a volume element in the real system, which must be simulated in the model system. The region

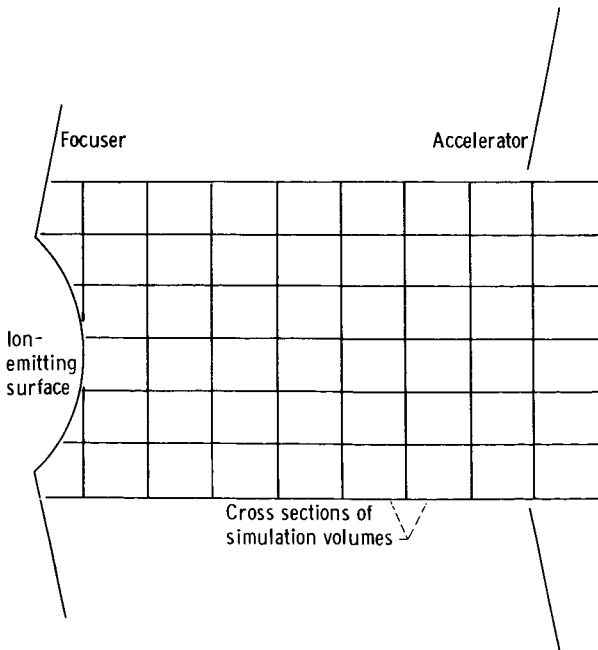


Figure 8. - Cross section of thruster showing cross sections of simulation volumes.

through which the beams of each system pass may be divided into a number of these volume elements (fig. 8); the elements are parallelepiped in shape, and those in the model system, called simulation volumes, are scaled replicas of those in the real system. If the integrated current through the elementary volume is denoted by I , equation (10) can be written

$$I = \frac{\sigma F^2}{\epsilon_o \alpha} Q_r \quad (11)$$

This current must be injected into the simulation volume in the electrolytic-tank analog from an external source. Since

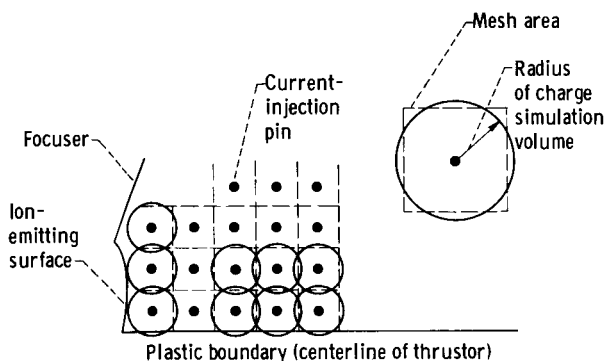


Figure 9. - Simulation of charge by cylinders representing parallelepipeds.

field measurements are taken at the surface of the electrolyte, the proper potential distribution must also occur at this surface. It has been empirically determined (ref. 3) that these conditions may be satisfied by injecting the current from a partially insulated pin protruding from the floor of the electrolyte tray. As shown in figure 9 the pins actually simulate the charge in the cylinders. If the cylinders

are equal in cross-sectional area to the parallelepipeds, however, a good simulation is obtained at the surface of the electrolyte. The determination of the appropriate value of the injection current I of equation (11) requires a knowledge of Q_r . The method used herein to calculate the values of Q_r differs considerably from previously reported methods and is a key factor in increasing the versatility of the Lewis Research Center analog.

To begin, consider the real thrustor and a scaled thrustor the size of the electrolyte model. The relation between the currents emitted from similar elemental areas of the emitters in the two thrustors is

$$J_r = C_1 J_f \quad (12)$$

where C_1 is a constant and J_f is the current in the scaled thrustor. The total current flow from the thrustors is divided into "stream tubes." Each stream tube of current flow originates from one of the elemental areas on the emitting surface. To consider space-charge-limited current flow, the currents flowing in a stream tube of either thrustor may be approximated by employing a technique described in reference 9 in connection with a digital computer program for solution of space-charge-flow problems. This technique is referred to as the "plane diode approximation." To determine these currents, an equipotential line close to the emitting surface is selected as shown in figure 10, and it is assumed that it forms a parallel-plate plane diode of separation ℓ_f with respect to each elemental area of the emitting surface. By using the mean value of ℓ_f , J_f is calculated for each stream tube from Child's law for space-charge-limited flow

$$J_f = C_2 V_f^{3/2} \frac{a_f}{\ell_f^2} \quad (13)$$

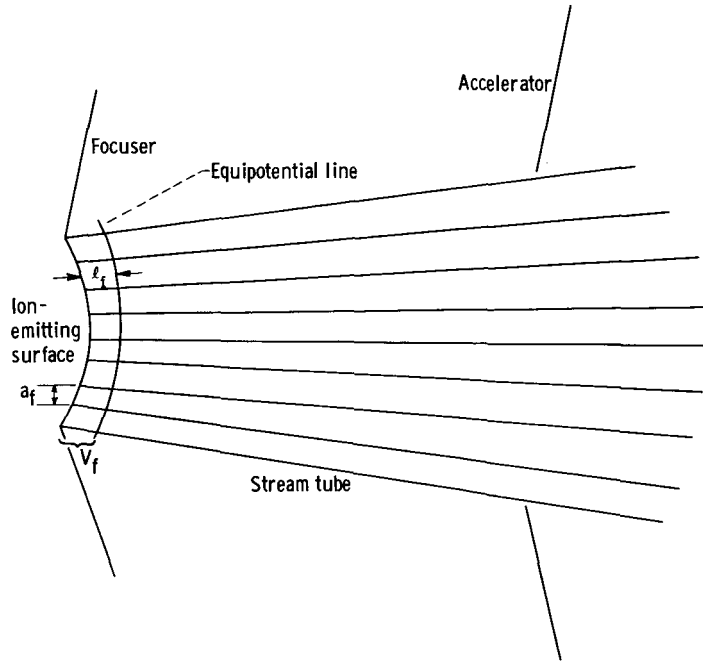


Figure 10. - Plane diode approximate method for determining current flowing in stream tubes.

where $C_2 = (4/9)\epsilon_0\sqrt{2\eta}$, V_f is the potential difference shown in figure 10, and a_f is the elemental area. Similarly

$$J_r = C_2 V_r^{3/2} \frac{a_r}{l_r^2} \quad (14)$$

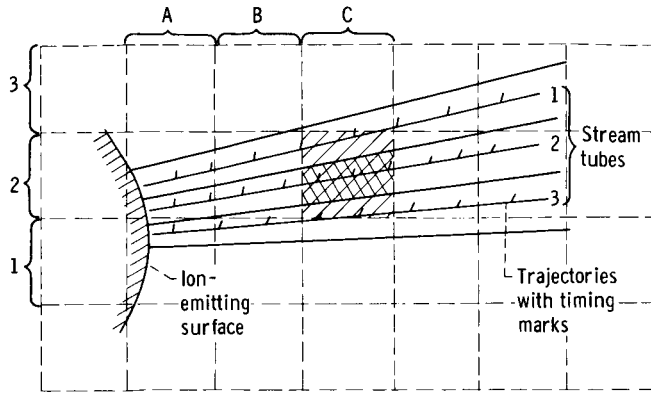
From equations (13) and (14) it follows that

$$J_r = \frac{V_r^{3/2}}{V_f^{3/2}} J_f \quad (15)$$

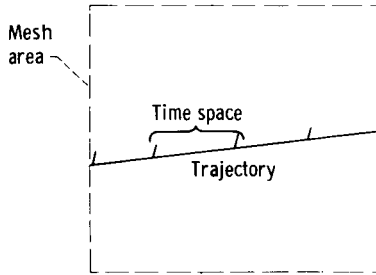
and the proportionality constant of equation (12) is therefore

$$C_1 = \left(\frac{V_r}{V_f} \right)^{3/2}$$

For each elementary simulation volume, summing over all the stream tubes in the volume gives



(a) Trajectories passing through mesh area (top view of volume element).



(b) Trajectory with superimposed timing marks. Number of time spaces in simulation volume, 4.

Figure 11. - Typical mesh area.

$$Q_r = \sum_i J_{r,i} t_i \quad (16)$$

where $J_{r,i}$ is the current in the i^{th} stream tube and t_i is the interval of time (measured in the real system) that the ions of the i^{th} tube remain in the simulation volume. In actual practice, of course, the smaller the elements of emitting area and the smaller the simulation volumes, the better the space-charge simulation will be. By using equation (15), equation (16) becomes

$$Q_r = \frac{V_r^{3/2}}{V_f^{3/2}} \sum_i J_{f,i} t_i \quad (17)$$

Now let $\beta = \tau_i/t_i$ where τ_i is the scaled time that the ions of the i^{th} stream tube spend in a simulation volume of the model-size thruster. The

value of β is determined from the scaling constants between the real and simulated thruster and will be discussed in the next section. Then, by substitution, equation (17) becomes

$$Q_r = \frac{V_r^{3/2}}{V_f^{3/2} \beta} \sum_i J_{f,i} \tau_i \quad (18)$$

In an actual case, the stream tubes are constructed so that the particle trajectories form the centerlines of the tubes (fig. 11(a)). Timing marks are superimposed on the trajectories at equal time intervals T . Thus, for any simulation volume, the number of time spaces in the simulation volume $N_{v,i}$ may be counted for each stream tube (fig. 11(b)). Multiplying $N_{v,i}$ by the time per space (T) yields τ_i for each stream tube. When only a portion of a stream-tube section passes through a charge simulation volume, the contribution to the charge in that volume is obtained by prorating on an area basis. For example, in figure 11(a) stream tube 2 contributes entirely to the charge in mesh 2C (double cross-hatched area). The prorating factor A_i is 1.0 for this case. Stream

tubes 1 and 3 contribute only partially to mesh 2C (single cross-hatched areas). Since

$$\tau_i = N_{v,i} T$$

using equation (18) results in equation (11) becoming

$$I = \frac{\sigma F^2 V_r^{3/2} T}{\epsilon_o \alpha V_f^{3/2} \beta} \sum_i J_{f,i} N_{v,i} A_i \quad (19)$$

Now α may be written as

$$\alpha = \frac{V_r}{V_f} F \quad (20)$$

By using this equation and the Child's law relation for the current flowing in a stream tube

$$J_{f,i} = \frac{4}{9} \epsilon_o \sqrt{2\eta} V_f^{3/2} \frac{a_{f,i}}{\ell_{f,i}^2} \quad (21)$$

equation (19) becomes

$$I = \frac{4 \sqrt{2} \eta^{1/2} \sigma F^{1/2} \alpha^{1/2} T V_f^{3/2} a_f}{9 \beta} \sum_i \frac{N_{v,i} A_i}{\ell_{f,i}^2} \quad (22)$$

The emitting area a_f may be taken outside the summation by requiring that all stream tubes be the same width. This is the basic equation resulting from the new technique used to evaluate space charge. The currents in the stream tubes are recalculated for each iteration. In the next section some of the parameters of equation (22) will be evaluated and a final form useful for computation will be presented.

Obtaining Working Equations for Analog

Before equation (1) can be solved in the analog computer, it is necessary to consider

scaling the problem and calibrating the analog. It is convenient to discuss calibration briefly at this point in connection with the evaluation of various parameters occurring in equation (22).

Consider the x-component of equation (1) written in terms of the real system

$$\frac{d^2 x_r}{dt^2} = -\eta E_{x, r}$$

Now

$$E_{x, r} = - \frac{\partial V_r}{\partial x_r} \quad (23)$$

or converting to the model-size thruster,

$$E_{x, r} = - \frac{\partial V_f}{\partial x_f} \alpha \quad (24)$$

Define

$$\frac{\partial V_f}{\partial x_f} = K_c \delta_{x, m} \quad (25)$$

where $\delta_{x, m}$ is a small potential difference measured between two closely spaced points in the electrolyte along the x-axis and K_c is a constant. Actually, $\delta_{x, m}$ is the signal input to the analog computer measured in the electrolyte by the two x-component sampling probes. Equation (1) then becomes

$$\frac{d^2 x_r}{dt^2} = \eta \alpha K_c \delta_{x, m} \quad (26)$$

If the time scaling ratio $\beta = \tau_i/t_i = d\tau_i/dt_i$ is used, equation (26) may be written as

$$\frac{d^2 x_r}{d\tau_i^2} = \frac{\eta \alpha K_c \delta_{x, m}}{\beta^2} \quad (27)$$

The relation between the distance variable x and the computer output in volts from equation (6) is

$$x_r = \frac{x_m}{F} = \frac{\bar{X}}{FS} \quad (28)$$

where \bar{X} is the distance variable expressed in volts and S is the plotting scale factor in volts per meter. Therefore,

$$\frac{d^2 \bar{X}}{d\tau_i^2} = \frac{FS \eta \alpha K_c \delta_{x, m}}{\beta^2} \quad (29)$$

All the components of the right side of equation (29) are constant for any given problem except $\delta_{x, m}$, so that

$$\frac{d^2 \bar{X}}{d\tau_i^2} = B \delta_{x, m} \quad (30)$$

where

$$B = \frac{\eta FS \alpha K_c}{\beta^2} \quad (31)$$

The significance of B in equation (30) is that it represents the overall gain of the signal $\delta_{x, m}$ that is fed to the computer. The value of B determines the plotting speed and is adjusted by a potentiometer until this speed is optimized (i. e., plotting too fast will create waves in the electrolyte and cause distortion; plotting too slow will allow small errors to multiply in the electronic integrators).

The y-components of the equations of motion are developed in exactly the same manner as the x-component. Therefore,

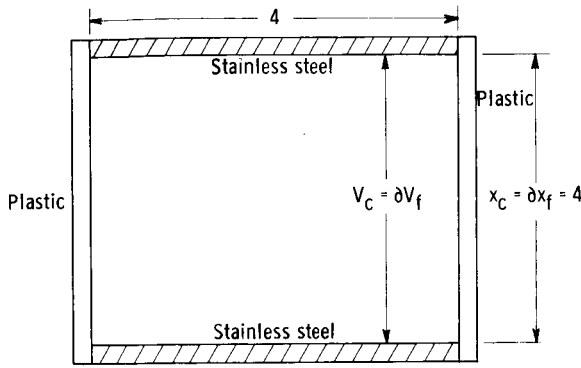


Figure 12. - Top view of calibration electrode unit. Height, 1.45 inches. (All dimensions in inches.)

$$\frac{d^2 \bar{Y}}{d\tau_i^2} = B \delta_{y, m} \quad (32)$$

In order to evaluate I in equation (22), it is necessary to obtain β . From equation (31),

$$\beta = \left(\frac{\eta F S \alpha K_c}{B} \right)^{1/2} \quad (33)$$

and from equation (25),

$$K_c = \frac{\partial V_f}{\partial x_f \delta_{x, m}} \quad (34)$$

In the calibration $\partial V_f / \partial x_f = V_c / x_c$ where V_c is the voltage across the calibration electrodes (see fig. 12), x_c is the distance between them, and $\delta_{x, m} = \delta_c$ is the signal fed to the computer from the sampling probes on the surface of the electrolyte between the electrodes, so that K_c may be evaluated from

$$K_c = \frac{V_c}{x_c \delta_c} \quad (35)$$

The values of the terms in equation (35) are the same for both x- and y-components. Finally, by substituting for β in equation (22) and by using equation (35), the current to be injected in a simulation volume of the model system is given by

$$I = \frac{4\sqrt{2}\sigma B^{1/2} T x_c^{1/2} \delta_c^{1/2} V_f^{3/2} a_f}{9V_c^{1/2} S^{1/2}} \sum_i \frac{N_{v, i} A_i}{\ell_{f, i}^2} \quad (36)$$

Equation (36) shows that the space-charge simulation current is independent of the scale of the models since F is contained only in B , which is an operationally determined constant. Once a converged solution is obtained for the trajectories, the current density for the solution may be calculated by using the plane diode approximation, by choosing

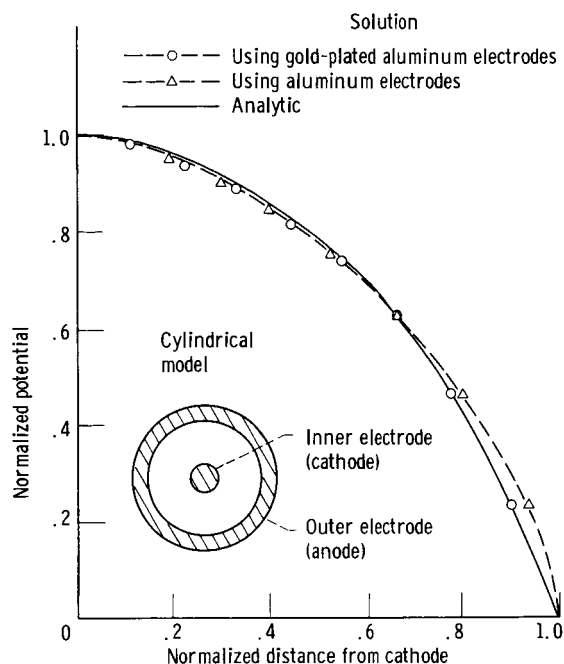


Figure 13. - Comparison of space-charge-limited-flow potential distributions between coaxial cylinders under different polarization effects.

the proper value for η , and by substituting the thruster voltages and dimensions desired. The generality of equation (36) is obvious since it applies to all two-dimensional configurations. Equation (36) will be referred to in the next section where some example solutions are discussed.

ILLUSTRATIVE EXAMPLES

Initial Test of Analog and Discussion of Solutions

A cylindrical diode model for which the analytic space-charge-limited flow results are known (ref. 10) was used to check the quality of the results obtained by the electrolytic-tank analog. Aluminum electrodes were used initially in this test because of their availability. They were then gold-plated to check the polarization effects. Comparison of the analytic with the analog space-charge-limited potential distributions is shown in figure 13 for the two different surface materials. Because some aluminum was exposed, the electrodes were very difficult to keep clean for more than a few minutes in the water.

For the gold-plated electrodes, which were the best, the maximum error in trajectory position for the test case was 3 percent where the error is defined as the trajectory

deviation from the analytic solution at its endpoint divided by the total trajectory length.




Some of the solutions to be presented in this section will be compared with solutions obtained from a digital computer program (ref. 9). The computer furnishes more detailed results for a final analysis. As will be shown in this section, though, the electrolytic tank analog is more versatile in initial studies. Once trends are established and the optimum electrode configuration is approached by using the electrolytic-tank analog, the more accurate digital program may be desired for the final stages of solutions.

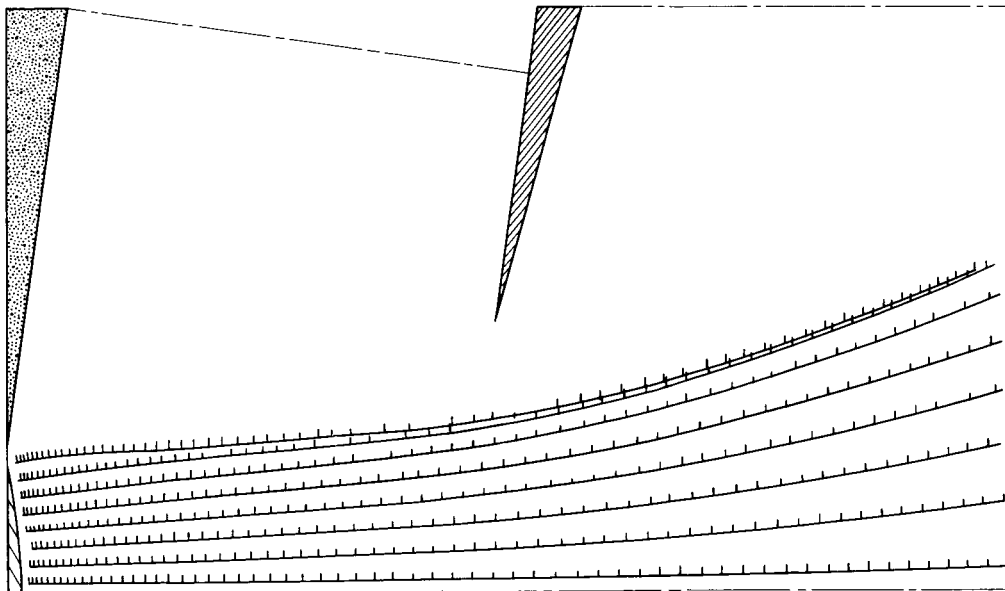
The two models to be discussed in this section are possible configurations for a contact-ionization type of electrostatic thruster. These configurations are based on the idealized design concepts given in reference 11.

Divergent-Flow Model

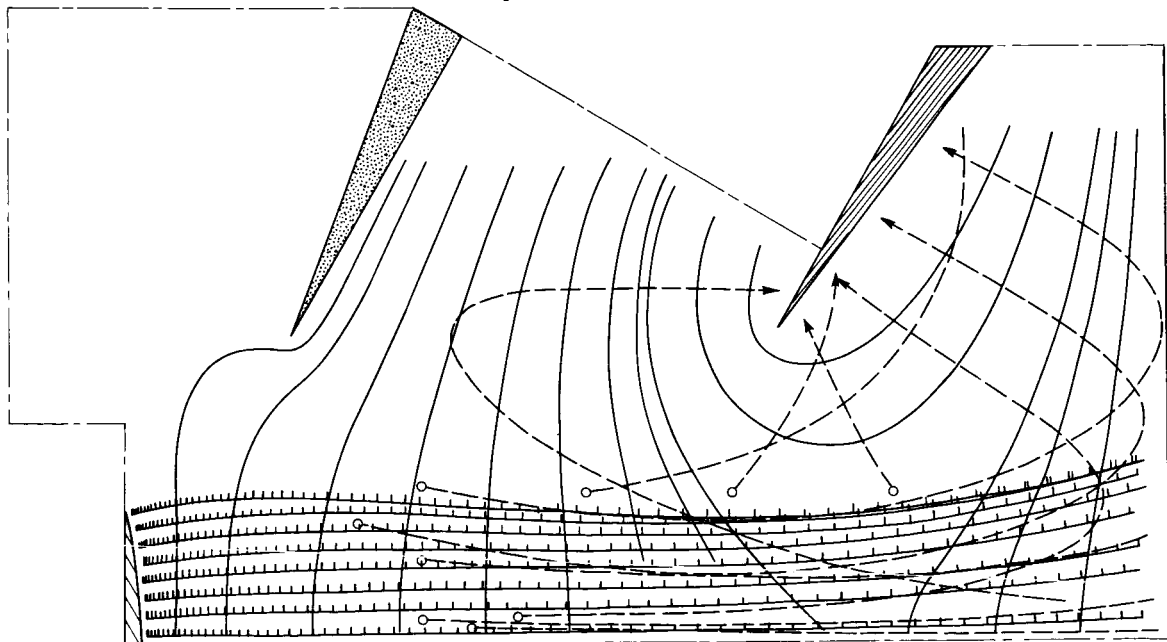
As discussed in reference 11, the divergent-flow concept has the promise of high current densities at the emitter and reduced densities in the area of critical charge exchange (aperture area). A model of the divergent-flow electrostatic thruster in the electrolytic tank is shown in figure 4 (p. 5). The space-charge-free solution is shown in figure 14(a). This solution is a starting point toward a practical design for the thruster. Although figure 14(a) shows only a space-charge-free solution of the model, it serves as a reference for studying configuration variations (e. g., the trend of the magnitude of the current density can be observed by noting the changes in position of an equipotential line near the emitting surfaces of various models). These variations are of interest for the purpose of improving the average current density possible from the thruster and focusing the beam more satisfactorily. A flat electrode downstream of the accelerator aperture is maintained at effectively zero potential (i. e., ground reference) to simulate an approximate exhaust beam neutralization plane. This in turn allows simulation of accel-decel operation of the model. In the configuration shown, the ratio used was $\varphi_A/\varphi_{\text{net}} = 3$ where φ_A is the difference between the emitter and the accelerator and φ_{net} is the net potential difference between the emitter and the ground.

An important factor that must be minimized in the design of a thruster is charge-exchange erosion of the accelerator (ref. 1). Charge exchange may occur when a fast moving ion collides with a slow neutral particle. After the collision the slow particle has acquired the charge and, depending on its originating position, may strike the electrodes, causing erosion and reduced thruster lifetime. As discussed in reference 2, the electrolytic tank analog is well suited for studying the charge-exchange ion trajectories and patterns of electrode erosion. Although charge-exchange studies made in a Laplace potential field do not directly apply to the final solution of a model, they may be used in the manner previously discussed to predict trends. Figures 14(b) to (d) show space-

- Typical point where charge exchange is assumed to occur
-  Focuser
-  Accelerator
-  Ion emitter
- Equipotential line
- - - Plastic boundary
- - - Charge-exchange ion trajectory
- - - Primary ion trajectory

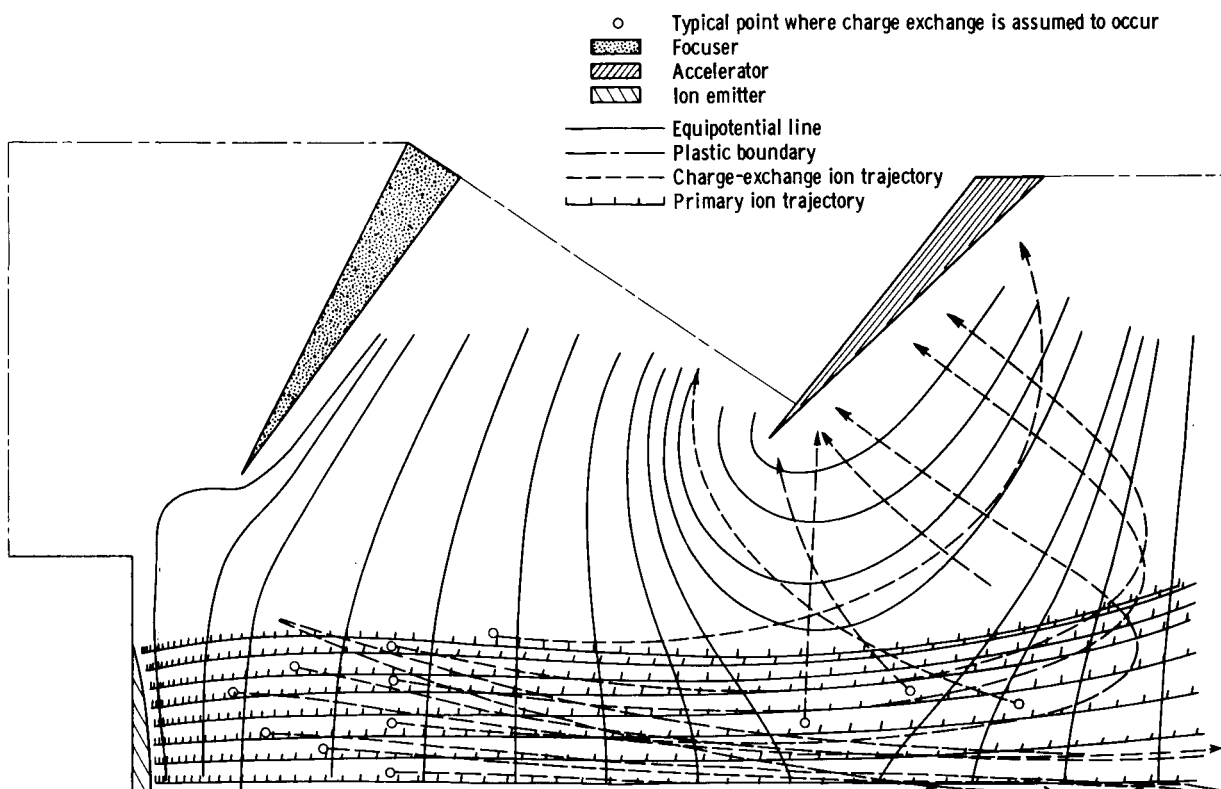


(a) Configuration 1.

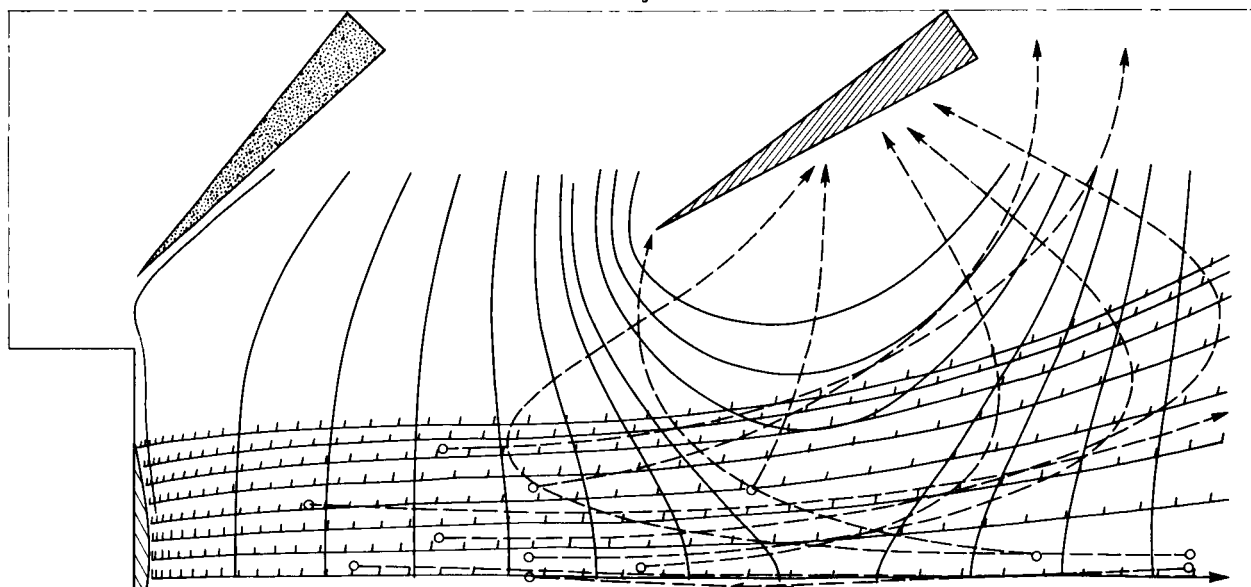


(b) Configuration 2.

Figure 14. - Divergent-flow configurations of space-charge-free solution in electrolytic tank. Focuser voltage in tank, 0 volt; accelerator voltage in tank, 6 volts; neutralization plane voltage in tank, 2 volts.

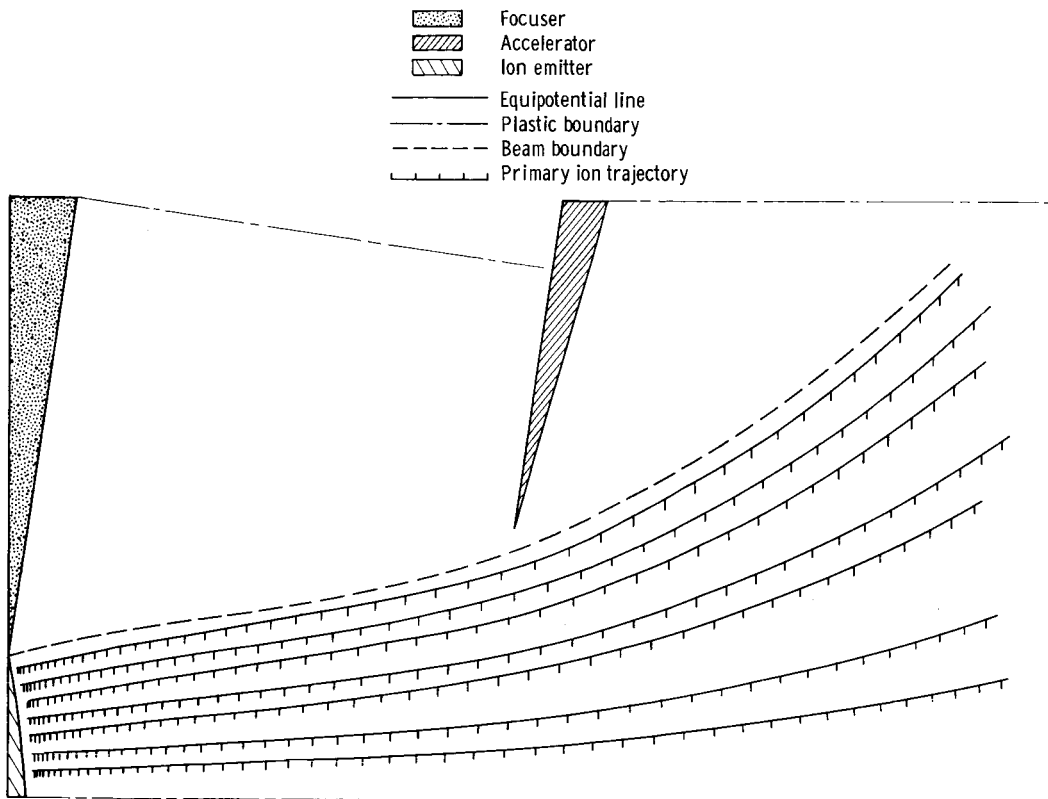


(c) Configuration 3.

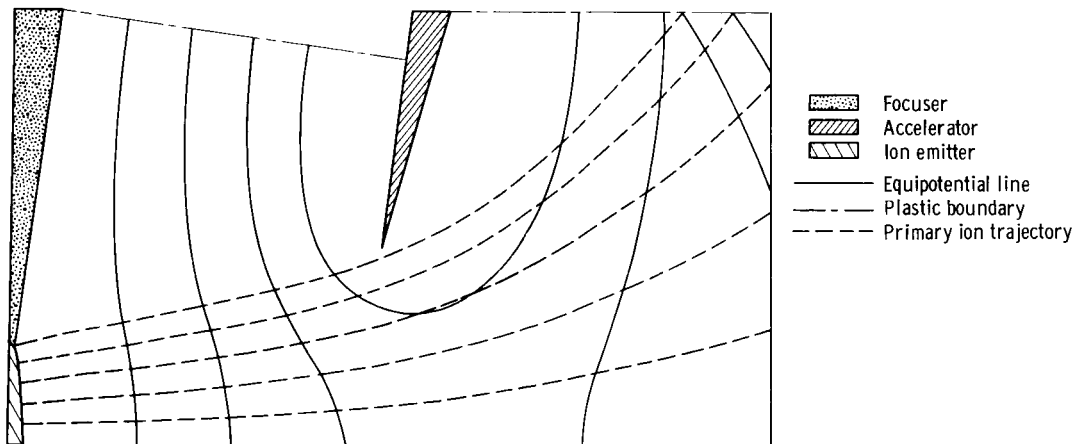


(d) Configuration 4.

Figure 14. - Concluded. Divergent-flow configurations of space-charge-free solution in electrolytic tank. Focuser voltage in tank, 0 volt; accelerator voltage in tank, 6 volts; neutralization plane voltage in tank, 2 volts.

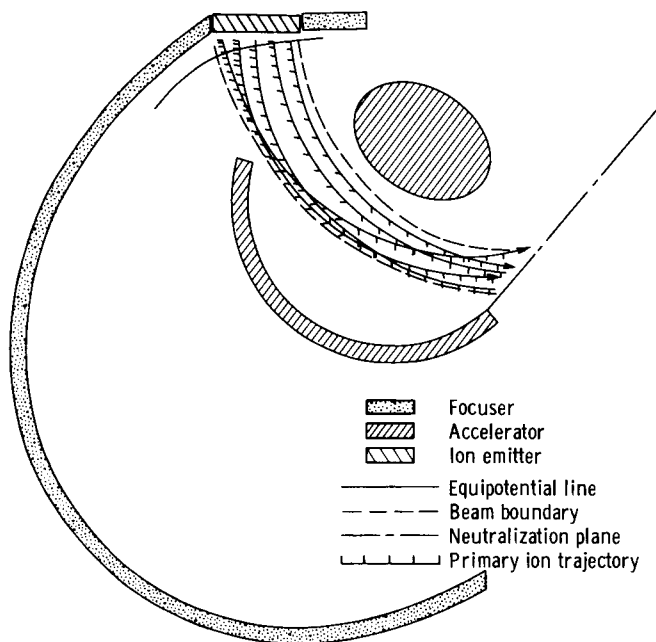


(a) Electrolytic tank. Average current density at ion-emitting surface, 91.5 amperes per square meter.

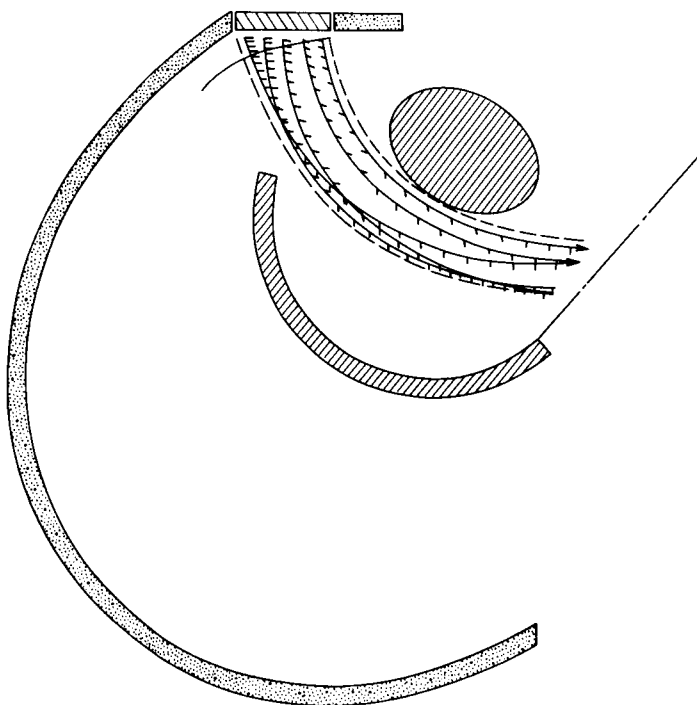


(b) Digital program. Average current density at ion-emitting surface, 83.4 amperes per square meter.

Figure 15. - Divergent-flow configuration 1 of space-charge-limited solutions. Focuser voltage: simulated, 1 kilovolt; in tank, 0 volt; accelerator voltage: simulated, -2 kilovolts; in tank, 6 volts; neutralization plane voltage: simulated, 0 kilovolt; in tank, 2 volts.



(a) Configuration 1 of space-charge-free solution. Average current density at ion-emitting surface, 159 amperes per square meter.

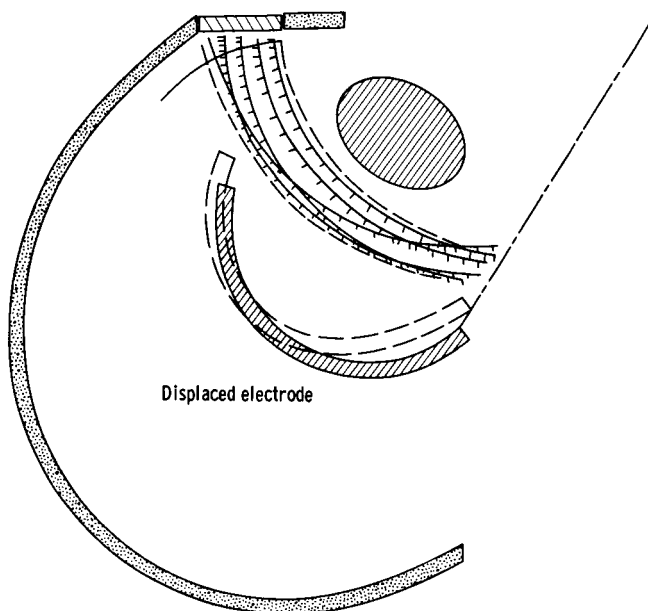


(b) Configuration 1 of space-charge-limited solution. Average current density at ion-emitting surface, 128 amperes per square meter.

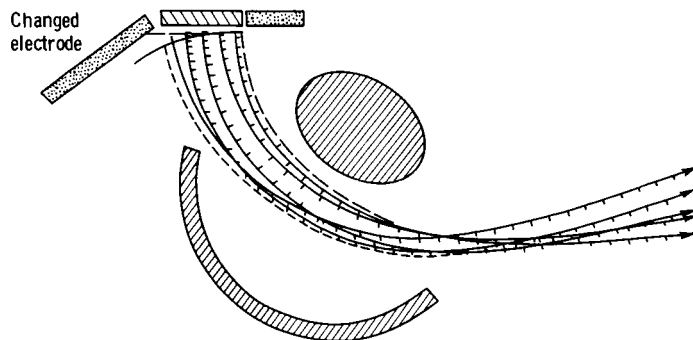
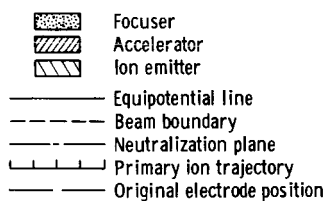
Figure 16. - Circular-flow configurations of various solutions in electrolytic tank. Focuser simulated voltage, 2.8 kilovolts; accelerator simulated voltage, -7.2 kilovolts; neutralization plane simulated voltage, 0 kilovolt.

charge-free solutions for some configuration variations of the original model. The dashed lines in figures 14(b) to (d) represent charge-exchange ion trajectories. The small circles are typical points where the charge exchanges are assumed to occur. The charge-exchange ions formed at these points start out with zero initial velocity. To obtain these trajectories, the field-sampling probe is positioned at the desired point and the trajectories are begun with no initial condition voltage (i. e., zero initial velocity). Many of these trajectories can be started at various points in the beam envelope so that a boundary may be established for the region where detrimental charge exchanges can occur. If the neutral efflux, primary ion density, and electric potential at the starting point are known, these trajectories provide a means for determining erosion patterns on the thruster electrode and calculating electrode life expectancy.

The space-charge-limited-flow solution for the model shown in figure 14(a) was obtained by using the electrolytic tank and also the digital computer program of reference 9. For the electrolytic-tank solution (fig. 15(a)), the emitter was divided into eight equal parts to establish the start of the stream tubes. The trajectories are started in the center of each stream tube so that the trajectory nearest the accelerator is not



(c) Configuration 2 of space-charge-free solution.



(d) Configuration 3 of space-charge-free solution. Average current density at ion-emitting surface, 175 amperes per square meter.

Figure 16. - Concluded. Circular-flow configurations of various solutions in electrolytic tank. Focuser simulated voltage, 2.8 kilovolts; accelerator simulated voltage, -7.2 kilovolts; neutralization plane simulated voltage, 0 kilovolt.

the beam boundary. The short dashed line represents this boundary. Figure 15(b) shows the digital solution for the model. In each case an accel-decel ratio (Φ_A/Φ_{net}) of 3 was used. A comparison between the two solutions can be made based on the amount of the aperture occupied by the beam envelope and the average emitter current density predicted. The two solutions differ in beam envelope size by 7.3 percent at the accelerator aperture. The lines traced in figure 15(b) represent stream-tube boundaries, while those in figure 15(a) represent the center-lines of the stream tubes. The predicted average current density at the emitter \bar{j}_e differs by 9.3 percent. The difference in predicted current density is probably due to inaccuracies in the measurement of $\ell_{f,i}$ (eq. (21)) from the electrolytic-tank trajectory plot.

Circular-Flow Model

As discussed in reference 11, the theoretical advantage of the circular-flow configuration is that the electrodes provide thermal shielding, thus reducing heat losses (fig. 16). With this configuration the hot ionizer does not have a direct line to space.

As in the previous case, the Laplace solution shown in figure 16(a) is the starting point for

analysis of the concept. Figure 16(b) shows the space-charge-limited-flow solution for this configuration. The space charge reduced the average current density of the emitter by 19.5 percent. This reduction is quite significant at high current densities. Also, figure 16(b) shows that the ion beam has been spread and shifted toward the elliptical accelerator electrode. The beam boundary barely misses the accelerator electrode. This close approach is undesirable because mechanical variations will probably result in impingement in the real thruster. The ratios of the voltages on the various electrodes for these cases are those discussed in reference 11.

The effect on the space-charge-free solution of displacing the circular arc electrode nearest the beam is shown in figure 16(c). As can be seen, this provides more clearance between the beam envelope and the electrodes. Variations that simplify the design of the thruster are also of interest. As an example, figure 16(d) shows a variation in which the large, curved outer electrode was replaced by a smaller, simpler one. The inner curved electrode was replaced to its original position. Also, the neutralization plane or simulated virtual ground was removed to observe the effect. The beam envelope produced by this variation is narrower than the previous configuration. The average predicted current density at the emitter increased 10 percent over the original model.

On several occasions during the solutions for the two thruster geometries discussed in this section, an iteration on the solution for both geometries was made in the same day. This illustrates the convenience of the removable-pin tray design and the versatility of this tank analog as an electrostatic-thruster design tool.

CONCLUDING REMARKS

The Lewis Research Center electrolytic tank analog has been used to analyze electrostatic-thruster geometries that present a particularly wide variety of two-dimensional space-charge-flow problems. The uniform spacing of the current-injection pins in this analog was found to provide a sufficiently accurate space-charge simulation for these configurations. This uniform spacing and the use of easily removable pins greatly reduced the time required to change models and make the high standard of cleanliness required for accurate solutions easier to maintain. The plane diode approximation method used for calculating the current flow in the stream tubes permitted generalization of the space-charge injection-current calculations, thereby further increasing the versatility of the analog. The circuitry developed for differencing, multiplying, and filtering the computer input signals increased the reliability and simplified the electronic requirements of the analog.

In the initial investigation of a problem, the space-charge-free solutions were found to be extremely useful guides to point out design deficiencies and establish trends for

reaching final electrode configurations and spacings in a space-charge field. More detailed solutions for the final stages of analysis are possible with digital computer programs.

Lewis Research Center,
National Aeronautics and Space Administration,
Cleveland, Ohio, January 26, 1965.

APPENDIX A

SYMBOLS

| | | | |
|---------------|--|-----------------------|--|
| A_i | fraction of stream-tube section within simulation volume | dv | element of volume |
| | | \bar{X}, \bar{Y} | coordinates, V |
| A_1, A_2 | amplitudes of sinusoidal function | x, y, z | Cartesian coordinates |
| a | emitting surface area, sq m | α | ratio of field intensities |
| B, C_1, C_2 | constants | β | time scaling factor |
| d | square wave distortion factor, V | δ | small potential difference, V |
| E | electric field intensity, V/m | ϵ_0 | permittivity of free space |
| F | dimensional scale factor | η | charge-mass ratio of ion, C/kg |
| I | space-charge simulation current, A | θ | phase difference |
| J | current, A | ρ | space-charge density, C/cu m |
| j | current density, A/sq m | σ | conductivity of electrolyte, mho/m |
| K_c | calibration constant | τ | scaled time, sec |
| l | linear distance | Φ_A | total accelerating potential, V |
| m | mass of ion, kg | Φ_{net} | net accelerating potential, V |
| N | number of time increments | ω | frequency, cps |
| P | square wave amplitude, V | Subscripts: | |
| P_r | starting point of trajectory | c | calibration |
| Q | electric charge, C | e | emitter |
| q | charge of ion, C | f | model-size thruster |
| S | plotter speed, V/m | i | i^{th} stream tube |
| ds | element of surface | m | analog model |
| T | time per increment, sec/space | r | real model |
| t | real time, sec | v | simulation volume |
| V | electric potential, V | 0 | initial value at starting point of trajectory (appendix B) |
| | | Superscript: | |
| | | $(\bar{})$ | average |

APPENDIX B

DETAILS OF INJECTION-PIN-CURRENT CALCULATIONS

Equation (36) is used to calculate the pin currents for space-charge simulation. The value of ℓ_f for each trajectory stream tube is measured by plotting an equipotential line near the emitter (e. g., see fig. 10, p. 13). The conductivity of the electrolyte is measured immediately before the pin-current calculations are made.

The first approximation to the pin-current value is too high because of the method employed to find the space-charge-limited flow (ref. 9). If the currents are decreased too much, a converged solution may require many additional iterations; if not enough, either a negative gradient is set up (an unrealistic condition) or the succeeding iterations will oscillate (i. e., trajectories will converge, diverge, etc.).

The following calculations are made from the sample plot shown in figure 17. The first number of simulation-volume time increments (from emitter to trajectory starting point P_r) in square A2 are determined by the quotient of the time it took the particle to travel from the emitter to point P_r divided by the time T between timing marks in seconds. Some typical values for the terms in equation (36) are the following:

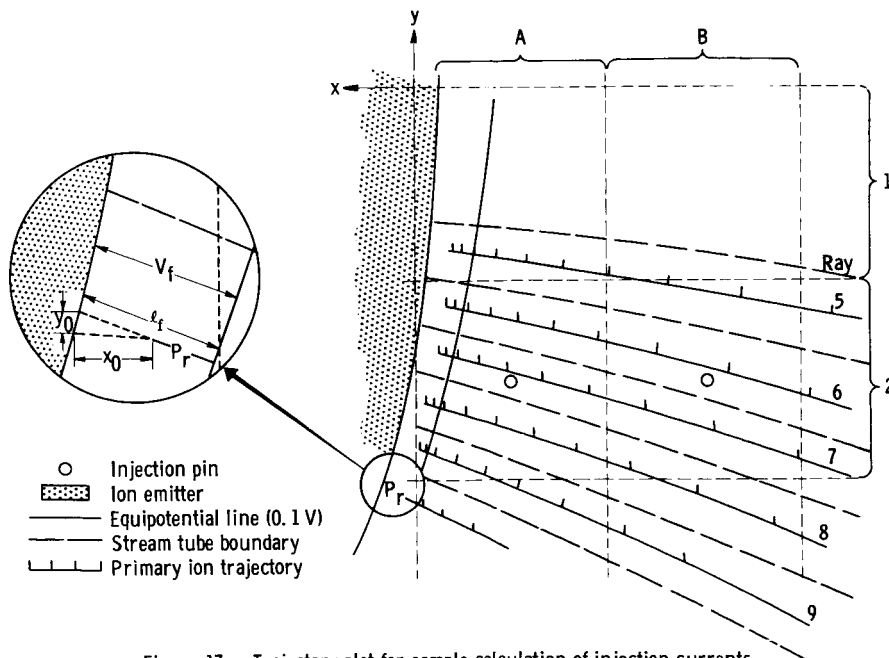


Figure 17. - Trajectory plot for sample calculation of injection currents.

| | |
|--|-----------------------|
| Conductivity of electrolyte, σ , mho/m. | 2.0×10^{-2} |
| Constant B. | 0.2 |
| Time per increment, T, sec/space | 0.5 |
| Distance between calibration electrodes, x_c , m. | 0.1016 |
| Small potential difference between calibration electrodes, δ_c , V. | 4.0 |
| Electric potential of model-size thruster, V_f , V | 0.1 |
| Emitter surface area of model-size thruster, a_f , sq m. | 3.68×10^{-4} |
| Calibration electric potential, V_c , V | 4.0 |
| Plotter speed, S, m/V | 197.0 |

so that equation (36) becomes

$$I = 7.3 \times 10^{-10} \sum_i N_{v,i} A_i \ell_{f,i}^{-2} \quad (B1)$$

Tables I to III illustrate the calculation of the injection current needed for the two pins shown in figure 17. Thus from table II and equation (B1), the pin currents for this sample iteration are those given in table III. The voltage dropped across the 10-kilohm series resistor must therefore be 3.51 volts for square A2 and 0.758 volt for square B2.

TABLE I. - STARTING POINTS, INITIAL VELOCITIES, AND $\ell_{f,i}^{-2}$

| Stream tube, i | Coordinate of starting point, x_0 | Initial velocity in x-direction, \dot{x}_0 | Time lapse to starting point, t_0 , sec | Coordinate of starting point, y_0 | Initial velocity in y-direction, \dot{y}_0 | Time lapse to starting point, t_0 , sec | Plane diode of separation, $\ell_{f,i}$, m | $\ell_{f,i}^{-2}$, m^{-2} |
|----------------|-------------------------------------|--|---|-------------------------------------|--|---|---|------------------------------|
| 5 | 0.0077 | -0.0072 | 2.2 | 0.0011 | -0.0009 | 2.2 | 10.0×10^{-3} | 1.00×10^4 |
| 6 | .0076 | -.0070 | 2.2 | .0014 | -.0011 | 2.3 | 9.0 | 1.23 |
| 7 | .0076 | -.0066 | 2.3 | .0016 | -.0012 | 2.4 | 8.0 | 1.56 |
| 8 | .0075 | -.0060 | 2.5 | .0019 | -.0013 | 2.6 | 7.0 | 2.04 |
| 9 | .0073 | -.0053 | 2.8 | .0022 | -.0013 | 2.8 | 6.5 | 2.37 |

TABLE II. - CALCULATION OF $\sum_i N_{v,i} A_i \ell_{f,i}^{-2}$

| Square | Stream tube, i | Number of time increments in i^{th} stream tube for volume V , $N_{v,i}$ | Prorating factor, A_i | $N_{v,i} A_i$ | $N_{v,i} A_i \ell_{f,i}^{-2}$ | $\sum_i N_{v,i} A_i \ell_{f,i}^{-2}$ |
|--------|----------------|---|-------------------------|---------------|-------------------------------|--------------------------------------|
| A2 | 5 | $(2.2/T) + 5.9$ | 0.15 | 1.21 | 1.21×10^4 | 48.15×10^4 |
| | 6 | $(2.2/T) + 6.1$ | .98 | 8.13 | 10.00 | ----- |
| | 7 | $(2.3/T) + 6.3$ | 1.00 | 8.60 | 13.42 | ----- |
| | 8 | $(2.5/T) + 6.6$ | .90 | 8.19 | 16.70 | ----- |
| | 9 | $2.8 + 6.8$ | .30 | 2.88 | 6.82 | ----- |
| B2 | 5 | 2.6 | 0.60 | 1.56 | 1.56×10^4 | 10.38×10^4 |
| | 6 | 2.6 | 1.00 | 2.60 | 3.20 | ----- |
| | 7 | 2.8 | .96 | 2.69 | 4.20 | ----- |
| | 8 | 2.8 | .25 | .70 | 1.42 | ----- |

TABLE III. - INJECTION

PIN CURRENTS FOR

TWO SAMPLES

| Square | Pin current, amp |
|--------|-----------------------|
| A2 | 3.51×10^{-4} |
| B2 | 7.58×10^{-5} |

APPENDIX C

EVALUATION OF VARIOUS ELECTRODE MATERIALS

The model electrode material must be nonreactive to the tap water. For this reason, brass and stainless steel were considered for the material. Brass is easily machined and has the desired electrical properties; however, it was found that with brass electrodes, distortion of the electric field occurred because of polarization at the interface of the electrode and the electrolyte. The extent of distortion of this kind can be measured by applying a square wave signal across the electrodes and reading the signal

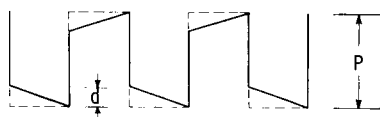


Figure 18. - Square wave obtained by use of brass electrodes.

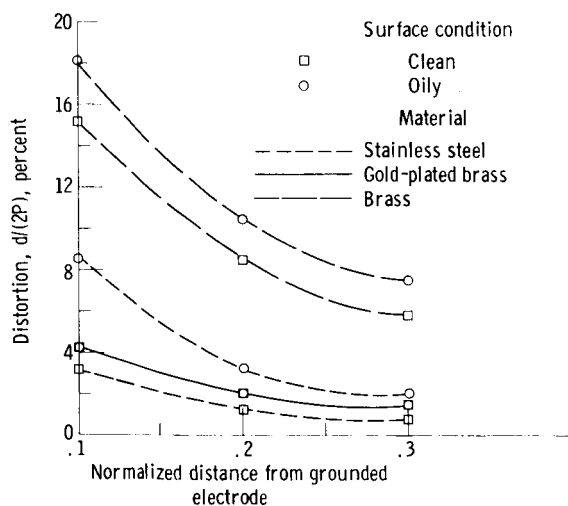


Figure 19. - Polarization effects using various electrode materials.

on an oscilloscope. The leading edge of the square wave shown in figure 18 indicates distortion. The relative distortion of various electrode materials and surface conditions, such as contamination caused by cleaning with alcohol or the presence of oil or fingerprints, can be compared by obtaining for each material and surface condition the ratio $d/2P$.

The test was conducted by using plane diode electrode configurations with 8 inches of spacing, and a 5.4-volt square wave was applied. The signal is measured with a probe immersed in the electrolyte between the electrodes at various distances from the grounded electrode. The distortion $d/2P$ is the percent reduction in the area under the square wave. The data from the comparison is shown in figure 19. It can be seen that best results were obtained with clean stainless steel. It is also noteworthy, how-

ever, that the gold-plated brass gave good results that were also very insensitive to surface cleanliness. These electrodes have advantages, but the gold-plating is time consuming and costly. Stainless steel is more difficult to fabricate but requires no surface preparation other than keeping the critical surfaces of the electrodes free from oils and fingerprints.

REFERENCES

1. Mickelsen, William R.; and Kaufman, Harold R.: Status of Electrostatic Thrusters for Space Propulsion. NASA TN D-2172, 1964.
2. Brewer, G.: On the Nature of Leakage Currents in Cesium Contact Ion Engines. Rept. No. 281, Hughes Res. Lab., Aug. 1963.
3. Hollway, D. L.: The Determination of Electron Trajectories in the Presence of Space Charge. Australian J. Phys., vol. 8, no. 1, Mar. 1955, pp. 74-89.
4. Van Duzer, T.; and Brewer, G. R.: Space-Charge Simulation in an Electrolytic Tank. J. Appl. Phys., vol. 30, no. 3, Mar. 1959, pp. 291-301.
5. Einstein, P. A.: Factors Limiting the Accuracy of the Electrolytic Plotting Tanks. British J. Appl. Phys., vol. 2, Feb. 1951, pp. 49-55.
6. Sander, K. F.; and Yates, J. G.: A New Form of Electrolytic Tank. Proc. Inst. Elec. Engrs., pt. C, vol. 104, no. 5, Mar. 1957, pp. 81-86.
7. Logan, B. F.; Welti, G. R.; and Sponsler, G. C.: Analogue Study of Electron Trajectories. Assoc. for Computing Machinery J., vol. 2, no. 1, Jan. 1955, pp. 28-41.
8. Terman, Frederick Emmons; and Pettit, Joseph Mayo: Electronic Measurements. Second ed., McGraw-Hill Book Co., Inc., 1952.
9. Hamza, Vladimir; and Richley, Edward A.: Numerical Solution of Two-Dimensional Poisson Equation: Theory and Application to Electrostatic-Ion-Engine Analysis. NASA TN D-1323, 1962.
10. Langmuir, I.; and Blodgett, Katherine B.: Currents Limited by Space-Charge Between Coaxial Cylinders. Phys. Rev., vol. 22, no. 4, Oct. 1923, pp. 347-356.
11. Lockwood, D. L.; Mickelsen, W. R.; and Hamza, Vladimir: Analytic Space-Charge Flow and Theoretical Electrostatic Rocket Engine Performance. Preprint 2400-62, ARS, 1962.